

# NO<sub>2</sub>-assisted molecular-beam epitaxy of Fe<sub>3</sub>O<sub>4</sub>, Fe<sub>3- $\delta$</sub> O<sub>4</sub>, and $\gamma$ -Fe<sub>2</sub>O<sub>3</sub> thin films on MgO(100)

F. C. Voogt\*

*Department of Physical Chemistry, Materials Science Centre, University of Groningen, Nijenborgh 4, 9747 AG, Groningen, The Netherlands*

T. Fujii†

*Department of Solid State Physics, Materials Science Centre, University of Groningen, Nijenborgh 4, 9747 AG, Groningen, The Netherlands*

P. J. M. Smulders and L. Niesen

*Department of Nuclear Solid State Physics, Materials Science Centre, University of Groningen, Nijenborgh 4, 9747 AG, Groningen, The Netherlands*

M. A. James and T. Hibma

*Department of Physical Chemistry, Materials Science Centre, University of Groningen, Nijenborgh 4, 9747 AG, Groningen, The Netherlands*

(Received 21 September 1998; revised manuscript received 5 April 1999)

We report on the molecular beam epitaxial growth of single-crystalline, stoichiometric Fe<sub>3</sub>O<sub>4</sub> and  $\gamma$ -Fe<sub>2</sub>O<sub>3</sub> films on MgO(100), using NO<sub>2</sub> as the oxidizing agent. Mössbauer spectroscopy on <sup>57</sup>Fe probe layers is used to determine accurately the stoichiometry of the films. It is found that also all intermediate nonstoichiometric Fe<sub>3- $\delta$</sub> O<sub>4</sub> phases can be obtained. The formation of the metastable compound  $\gamma$ -Fe<sub>2</sub>O<sub>3</sub> clearly demonstrates the large oxidizing power of NO<sub>2</sub>. Although the shape anisotropy dictates that the zero-field magnetization direction should lie entirely in the plane of the film, this is never observed. Stoichiometric Fe<sub>3</sub>O<sub>4</sub> has large out-of-plane components and only in the case of highly oxidized Fe<sub>3- $\delta$</sub> O<sub>4</sub> does the magnetization approach the film plane. Upon further oxidation to stoichiometric  $\gamma$ -Fe<sub>2</sub>O<sub>3</sub>, however, it rotates back, and finally becomes almost completely perpendicular to the plane of the film. Furthermore, in the case of (near-) stoichiometric Fe<sub>3</sub>O<sub>4</sub>, the magnetizations of the *A* and *B* sublattices are not completely coupled antiparallel. On average, the magnetization of the *B* site ions is 4° closer to the film plane than the magnetization of the *A* site ions. All the as-grown films exhibit a ( $\sqrt{2} \times \sqrt{2}$ )R45° surface reconstruction, independent of the stoichiometry. Using simple electrostatic considerations, we propose three possible surface terminations: a half-filled *A* layer, a *B* layer with oxygen vacancies and a *B* layer with hydroxyl groups. Upon annealing, the ( $\sqrt{2} \times \sqrt{2}$ )R45° reconstruction irreversibly transforms to a 3×1 reconstruction, caused by Mg outdiffusion from the substrate. Strong reflection high-energy electron diffraction intensity oscillations give direct, unambiguous evidence that Fe<sub>3</sub>O<sub>4</sub> has a two-dimensional layer-by-layer growth mode over the entire temperature range studied, i.e., from 273 to 723 K, guaranteeing atomically flat surfaces and interfaces in multilayer structures. The largest oscillations are obtained on *ex situ* cleaved, UHV-annealed MgO(100) substrates, or on *in situ* annealed Fe<sub>3</sub>O<sub>4</sub>/MgO(100) films. Deposition above ~700 K is accompanied by rapid Mg outdiffusion.

[S0163-1829(99)01539-8]

## I. INTRODUCTION

Of all known iron oxides, magnetite, Fe<sub>3</sub>O<sub>4</sub>, exhibits by far the most interesting properties. This is due to the presence of Fe cations in two valence states: as ferrous Fe<sup>2+</sup> and ferric Fe<sup>3+</sup> ions, distributed over tetrahedral *A* and octahedral *B* sites. Fe<sub>3</sub>O<sub>4</sub> crystallizes in the inverse spinel structure, which has a slightly distorted cubic close packed lattice of O<sup>2-</sup> anions as its basis. The lattice constant is 0.83963 nm.<sup>1</sup> From an ionic point of view, magnetite can be written as Fe<sub>A</sub><sup>3+</sup>[Fe<sup>3+</sup>Fe<sup>2+</sup>]<sub>B</sub>O<sub>4</sub><sup>2-</sup>, indicating that half of the Fe<sup>3+</sup> ions occupy one eighth of the available tetrahedral sites, whereas the other ferric ions, together with an equal amount of Fe<sup>2+</sup> ions, occupy half of the octahedral sites. The octahedral sites containing the Fe ions are connected in strings running in all  $\langle 110 \rangle$  directions.

One well-known property of Fe<sub>3</sub>O<sub>4</sub> is the high conductivity at room temperature, caused by a rapid electron hopping

between the Fe<sup>2+</sup> and Fe<sup>3+</sup> ions in these octahedral strings. When cooling down through the Verwey transition temperature *T<sub>V</sub>*, being about 120 K in bulk crystals, the electron hopping freezes out, leading to an ordered array of Fe<sup>2+</sup> and Fe<sup>3+</sup> ions with static charges. Despite extensive research over the last 50 years, this transition is still not fully understood.<sup>2</sup> Furthermore, Fe<sub>3</sub>O<sub>4</sub> is a ferrimagnet with a Curie temperature *T<sub>C</sub>* of 858 K.<sup>3</sup> The magnetism arises from the localized magnetic moments of the Fe ions. The *A* and *B* sublattices couple antiferromagnetically via superexchange, giving a net magnetic moment of ~4  $\mu_B$  per formula unit Fe<sub>3</sub>O<sub>4</sub>. This is the magnetic moment ( $g\mu_B S$  with  $S=2$ ) of the *B* site Fe<sup>2+</sup> ion, since the 5  $\mu_B$  moments of the Fe<sup>3+</sup> ions in *A* and *B* sites are opposite and cancel each other out.

With the advances in thin film growth techniques over the last two decades, it has become possible to deposit epitaxial films of this interesting material on single-crystalline substrates, and to study a variety of novel properties in artificial

multilayer structures, such as magnetic interlayer coupling,<sup>4</sup> exchange biasing<sup>5</sup> and the possibility of a perpendicular magnetic surface anisotropy.<sup>6</sup> Recent interest in Fe<sub>3</sub>O<sub>4</sub> films comes from the field of spin-polarized transport.<sup>7</sup> As an example of an application, we mention the so-called “spin-valve” devices.<sup>9</sup> The spin-polarized conductivity in Fe<sub>3</sub>O<sub>4</sub>, together with short-range hopping and the high-ordering temperature, gives this material intrinsic advantages over the presently employed metallic materials.

So far, most thin film growth studies have been focused on Fe<sub>3</sub>O<sub>4</sub>, due to its magnetic and electrical properties, and to a lesser extent on hematite,  $\alpha$ -Fe<sub>2</sub>O<sub>3</sub>. However, besides stoichiometric Fe<sub>3</sub>O<sub>4</sub>, there is a whole range of isostructural compounds, i.e., the nonstoichiometric Fe<sub>3- $\delta$</sub> O<sub>4</sub> and stoichiometric  $\gamma$ -Fe<sub>2</sub>O<sub>3</sub> phases. These phases have remained relatively unexplored. Maghemite,  $\gamma$ -Fe<sub>2</sub>O<sub>3</sub>, is a metastable compound, and very closely related to the stable phase magnetite. In fact, it is magnetite, but with all Fe<sup>2+</sup> ions oxidized to Fe<sup>3+</sup>. The lattice constant is 0.8352 nm.<sup>1</sup> To maintain charge neutrality, vacancies are introduced on the B site sublattice.<sup>10</sup> Thus, instead of  $\gamma$ -Fe<sub>2</sub>O<sub>3</sub>, one may write Fe<sub>2.67</sub>O<sub>4</sub>, or Fe<sub>A</sub><sup>3+</sup>[Fe<sub>5/3</sub><sup>3+</sup>□<sub>1/3</sub>]<sub>B</sub>O<sub>4</sub>, where □ indicates an octahedral vacancy. The intermediate Fe<sub>3- $\delta$</sub> O<sub>4</sub> phases can be considered as homogeneous solid solutions of Fe<sub>3</sub>O<sub>4</sub> and  $\gamma$ -Fe<sub>2</sub>O<sub>3</sub>, with the number of vacancies per formula unit,  $\delta$ , varying continuously from zero for stoichiometric Fe<sub>3</sub>O<sub>4</sub> up to one third for stoichiometric  $\gamma$ -Fe<sub>2</sub>O<sub>3</sub>. Because of the absence of Fe<sup>2+</sup> ions, electron hopping is no longer possible in maghemite making the material an insulator. On the other hand, it is still a ferrimagnet, with a magnetic moment of  $\sim \frac{2}{3} \times 5 = 3\frac{1}{3} \mu_B$  per formula unit. Maghemite can be obtained by moderate annealing of Fe<sub>3</sub>O<sub>4</sub> in air at  $\sim 575$  K.<sup>11</sup>

In this paper, we will show that we can prepare all these phases as epitaxial films, with an accurate control of the stoichiometry. We use molecular-beam epitaxy (MBE), i.e., the evaporation of Fe onto a substrate in an ultrahigh vacuum (UHV) environment, to prepare the films. By simultaneously exposing the metal deposits to an oxidizing agent, oxide films are formed. One key aspect of our work is a precise determination of the stoichiometry of the samples. To our knowledge, the only studies entirely dedicated to determine the stoichiometry of MBE-grown Fe<sub>3</sub>O<sub>4</sub> layers are those by Fontijn *et al.*<sup>12,13</sup> These authors used magneto-optical Kerr (MOKE) spectroscopy. Furthermore, Fujii *et al.* have used Mössbauer spectroscopy to verify the formation of stoichiometric Fe<sub>3</sub>O<sub>4</sub> films.<sup>14,15</sup> Here, we will augment the use of Mössbauer spectroscopy, and apply it on <sup>57</sup>Fe probe layers to identify all possible phases.

The pioneering work on epitaxial MBE-grown Fe<sub>3</sub>O<sub>4</sub> films has been performed by Bando and co-workers, using molecular O<sub>2</sub> as the oxidizing agent.<sup>14-17</sup> They found that the nature of the iron oxide films was determined by the choice of substrate, i.e., MgO(100) for Fe<sub>3</sub>O<sub>4</sub>(100) and  $\alpha$ -Al<sub>2</sub>O<sub>3</sub>(001) for  $\alpha$ -Fe<sub>2</sub>O<sub>3</sub>(001) or Fe<sub>3</sub>O<sub>4</sub>(111), and by the relative amounts of chemisorbed O<sub>2</sub> molecules and condensed Fe atoms; with the chemisorption of O<sub>2</sub> in turn being affected by the substrate temperature,  $T_{sub}$ .<sup>15,16</sup> In general, the most oxidized phases were obtained at the highest O<sub>2</sub> partial pressures and lowest  $T_{sub}$  values. Similar results were later obtained by other researchers; see Refs. 18 and 19.

A second key aspect of our work is that nitrogen dioxide, NO<sub>2</sub>, is used as the oxidizing agent. The above studies by Bando *et al.* showed that, with molecular O<sub>2</sub>, only stoichiometric Fe<sub>3</sub>O<sub>4</sub> and partially oxidized Fe<sub>3- $\delta$</sub> O<sub>4</sub> with  $\delta \leq 0.06$  can be obtained on MgO(100).<sup>15</sup> Since it is our aim to prepare all iron oxide phases, a stronger oxidizing agent is needed. Some research groups have studied the use of activated forms of O<sub>2</sub>, such as ozone O<sub>3</sub> (Ref. 20) or oxygen plasma.<sup>21</sup> Here, we use NO<sub>2</sub>. This gas has already successfully been applied in the growth of high- $T_C$  superconducting oxide films,<sup>22</sup> NiO, CoO, and Co<sub>3</sub>O<sub>4</sub> films on MgO(100) (Ref. 23) and  $\alpha$ -Fe<sub>2</sub>O<sub>3</sub> films on  $\alpha$ -Al<sub>2</sub>O<sub>3</sub>(001).<sup>24</sup> A major, practical advantage is that the as-bought NO<sub>2</sub> is directly ready for use; no plasma or ozone generators are needed.

The studies by Peacor *et al.*<sup>23</sup> showed that NO<sub>2</sub> is a very efficient oxidizing agent: only small doses are needed to fully oxidize the metal deposits. Consequently, the background pressure could be maintained in the near-UHV region, i.e.,  $10^{-6}$ – $10^{-5}$  Pa. Normally, the metal is evaporated in a high background pressure of O<sub>2</sub> (up to  $\sim 10^{-3}$  Pa). In contrast, we provide both the metal and the oxidizing agent in the form of molecular beams. Therefore, not only the deposition, but also the oxidation process can abruptly be stopped. Using a background pressure of O<sub>2</sub>, the samples will inevitably remain for some time in an oxidizing environment after closing the Fe source. This can lead to post oxidation. Furthermore, the ability to deposit thin films under near-UHV conditions opens up the possibility to perform systematic *in situ* studies on freshly prepared, clean surfaces with scanning tunneling microscopy (STM), x-ray photoelectron spectroscopy (XPS), and other surface sensitive techniques.

## II. EXPERIMENT

### A. Thin-film growth

All samples have been prepared in a standard UHV MBE system, equipped with facilities for XPS, Auger electron spectroscopy (AES), reflection high-energy electron diffraction (RHEED), and low-energy electron diffraction (LEED). The films have been grown on MgO(100) substrates. The lattice constants of Fe<sub>3</sub>O<sub>4</sub> and  $\gamma$ -Fe<sub>2</sub>O<sub>3</sub> are nearly twice that of MgO, 0.42112 nm,<sup>1</sup> resulting in small lattice mismatches of  $-0.31$  and  $-0.84$  %, respectively. In our experiments, we have used *ex situ* cleaved MgO(100) substrates. Since MgO has an excellent cleavage along the {100} planes, high-quality substrates can be obtained by simply cleaving platelets with typical dimensions of  $10 \times 10 \times \sim 0.5$  mm<sup>3</sup> from a single-crystal block. As MgO is very sensitive to water vapor in the air, the crystals were cleaved in a dry environment, as shortly as possible before using them. It is believed that water reacts with MgO to form patches of Mg(OH)<sub>2</sub>, leaving MgO vacancies behind.<sup>25</sup> The substrates were glued on stainless steel plates with Ag paint and fixed with Ta clamps. After allowing the paint to dry for 1 day in an oven at 425 K, the samples were introduced into the UHV system via a load lock. Subsequently, they were cleaned by annealing for 2 to 3 hours at 975 K in  $1 \times 10^{-4}$  Pa O<sub>2</sub>. This procedure invariably led to well-ordered and atomically clean surfaces, as determined by RHEED, LEED [see Figs. 5(a) and 6(a)], AES and XPS. Annealing at higher temperatures and/or for

longer periods resulted in the segregation of Ca impurities from the bulk of the MgO to the surface, in agreement with observations by Gajdardziska-Josifovska *et al.*<sup>26</sup>

Oxide films were grown by depositing Fe from effusion cells, with the simultaneous oxidation of the metal deposits by a beam of NO<sub>2</sub> particles. The substrate temperature was set at 525 K. As will be shown below, this temperature is high enough to ensure a good layer-by-layer growth mode, while it is still safely below the onset of interdiffusion at the MgO/Fe<sub>3</sub>O<sub>4</sub> interface, i.e., ~625–675 K.<sup>27</sup> The gas delivery system consists of a small buffer volume into which the oxidizing agent is fed via a leak valve. From the buffer volume, the gas is free to flow through a 35-cm long stainless steel tube, with a diameter of 1 cm. The tube makes an angle of 60° with the substrate surface normal, and the opening is at a distance of 10 cm from the sample. Although the exact flux of oxidizing particles at the substrate surface can only be estimated, it is proportional to the buffer volume pressure  $P_{buf}$ . Therefore, this parameter was varied in order to obtain oxides with different stoichiometries.  $P_{buf}$  was measured with a Baratron capacitance manometer; in units of mTorr. The variation in  $P_{buf}$  during deposition was  $\leq 1\%$ .

The <sup>57</sup>Fe (enriched up to 95%) was evaporated from a cell with a source-substrate distance of 10 cm, while natural Fe was evaporated from a cell at a distance of 23 cm. Fluxes were measured by moving the quartz crystal microbalance in the position of the MgO substrate. Both fluxes were set at 0.13 nm min<sup>-1</sup>, which required temperatures around 1450 and 1575 K for the <sup>57</sup>Fe and natural Fe cells, respectively. Deposition onto the substrate could be started and stopped abruptly by opening and closing a shutter over the opening of the crucible. RHEED was used to monitor the surface evolution of the films (see Sec. III C). Since MgO is a very good insulator with a band gap of ~8 eV, the substrates tended to charge. To overcome this problem, an auxiliary floodgun was added to the setup.<sup>28</sup> This floodgun consisted of a filament at a distance of ~5 cm from the manipulator, which emitted low-energy electrons (~10<sup>2</sup> eV).

The <sup>57</sup>Fe magnetite probe layer had a thickness of 20.0 nm. Thicknesses were calibrated by monitoring the RHEED intensity oscillations during deposition (see Sec. III D). We used the assumption that each oscillation corresponded to the formation of one new atomic monolayer (ML), with a thickness of 0.21 nm (one fourth of the unit cell height). Film thicknesses were also measured independently with x-ray diffraction (XRD). The thicknesses thus obtained were in good agreement with our RHEED estimations, justifying the assumption.<sup>13,29</sup> Furthermore, the formation time of 1 ML of iron oxide was also in agreement with the value  $J_{Fe}$ , as measured with the quartz crystal microbalance. A flux of 0.13 nm min<sup>-1</sup> corresponds to  $1.8 \times 10^{17}$  Fe particles m<sup>-2</sup> s<sup>-1</sup>, and since 1 ML of Fe<sub>3</sub>O<sub>4</sub>(100) contains  $8.5 \times 10^{18}$  Fe particles m<sup>-2</sup>, one would expect a ML formation time of 46 s. This was in good agreement with the observed RHEED intensity oscillation periods.

Since the Mössbauer measurements were performed *ex situ*, the samples had to be transported through air after preparation. To avoid any post-oxidation of the <sup>57</sup>Fe probe layer at this stage, a cap layer was grown for protection. This cap layer consisted of magnetite, grown with the same NO<sub>2</sub> flux and with natural Fe. Therefore, it had the same degree of

oxidation, but was Mössbauer inactive. Its thickness was 5.0 nm, which is large enough to protect the inner <sup>57</sup>Fe probe layer. Previous studies on Fe<sub>3</sub>O<sub>4</sub>/MgO(100) films have indicated that post-oxidation only affects the outer few atomic monolayers (~0.5 nm).<sup>30</sup> A layer, identical to the cap layer, was inserted as a buffer between the <sup>57</sup>Fe probe layer and the MgO(100) substrate. The purpose of this buffer layer was to eliminate any effects of interdiffusion, even though  $T_{sub}$  was already low enough. Thus, all films had a total thickness of 30.0 nm. A series of 18 samples in total has been made with NO<sub>2</sub>, whereby  $P_{buf}$  was varied from 0.75 to 10.00 mTorr. For comparison, one sample has been made with molecular O<sub>2</sub> as the oxidizing agent ( $P_{buf} = 10.00$  mTorr, resulting in a background pressure of  $1 \times 10^{-4}$  Pa). Finally, one sample was subsequently annealed for 2 days at 575 K in a flow of 1 atm O<sub>2</sub>, in order to fully convert it to the maghemite  $\gamma$ -Fe<sub>2</sub>O<sub>3</sub> phase.<sup>11</sup>

## B. Characterization

The composition of the samples was analyzed *in situ* with XPS and AES. A detailed analysis of the XPS Fe 2p core level and valence-band spectra has already been published in this journal.<sup>31</sup> It was found that all Fe<sub>3</sub>O<sub>4</sub> to  $\gamma$ -Fe<sub>2</sub>O<sub>3</sub> films are pure oxides, i.e., no nitrogen could be detected. Only when very low doses of NO<sub>2</sub> ( $P_{buf} \leq 0.60$  mTorr) are applied does nitrogen become incorporated into the crystal lattice. Such oxy-nitrides have the rocksalt structure of wustite, Fe<sub>1-x</sub>O.<sup>32–34</sup>

The Mössbauer spectra were measured in the conversion electron (CEMS) mode. Two setups were employed, i.e., a home-built high-vacuum system with channel plates, and a simpler one using a standard acetone-filled gas detector. In both cases, the velocity scale of the spectra was calibrated with an  $\alpha$ -Fe foil. The relative accuracy of the velocity calibration, which is determined by the temperature dependence of the magnetic field at the pick-up coil within the Mössbauer drive system, is estimated as  $\sim 10^{-3}$ .

The structural quality of the films has been assessed previously with XRD and Rutherford backscattering (RBS).<sup>29,32–35</sup> RBS measurements on Fe<sub>3</sub>O<sub>4</sub> (see Fig. 1) and  $\gamma$ -Fe<sub>2</sub>O<sub>3</sub> thin films typically show minimum yields in the main low-index channeling directions of 5 to 10 %. These values are slightly higher than the minimum yields measured on bare MgO(100) substrates, i.e., 25 to 3%. This indicates a high-structural quality of the films, although there are some defects. Probably, these defects are associated with antiphase boundaries between crystallographic domains. The latter are an inherent consequence of the nucleation process.<sup>7,8</sup> Apart from these defects, the films are single crystalline: XRD measurements show diffraction peaks that are as narrow as those of the substrate. All films grow (100)-oriented on MgO(100), with their  $\langle 100 \rangle$  axes aligned parallel to those of the substrate. Furthermore, they grow fully coherently (or pseudomorphically). The in-plane lattice constants of the films are slightly expanded to match that of the MgO substrate, resulting in small tetragonal film distortions. The observed high-structural quality is in complete agreement with work from other groups.<sup>21,36–38</sup> It is a reflection of the very similar fcc oxygen sublattices in the rocksalt and spinel structures, making MgO an almost ideal template for the

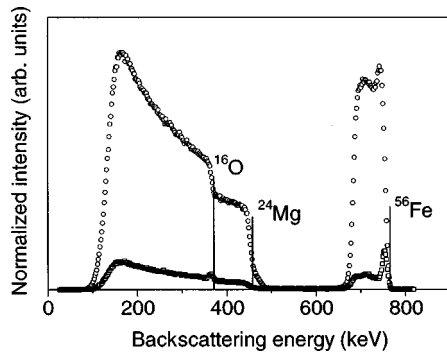


FIG. 1. RBS spectra of 1 MeV He ions scattered from a 30.0 nm thick magnetite  $\text{Fe}_3\text{O}_4$  film deposited on  $\text{MgO}(100)$  at 523 K. Two incident ion beam directions were used: a direction parallel to the  $[111]$  crystal axis (squares), and a direction with the beam tilted away from this axis. The small surface peaks indicate that the latter direction was not ideally random. Vertical lines indicate the positions of the edges of the three elements involved. The minimum channeling yield for Fe in the subsurface region is  $6 \pm 1\%$ .

epitaxial growth of  $\text{Fe}_3\text{O}_4$  to  $\gamma\text{-Fe}_2\text{O}_3$  thin films. The oxygen anion sublattice is continuous over the substrate/film interface; the  $\text{MgO}$  and the spinel lattices only differ in the occupation of the cation sites.

### III. RESULTS AND DISCUSSION

#### A. Mössbauer spectra

The stoichiometry determination with Mössbauer spectroscopy is based upon the rapid electron hopping process at room temperature. Since this hopping process is much faster than the lifetime of the excited  $^{57}\text{Fe}$  nucleus, the  $B$  site ions appear as one average “ $\text{Fe}^{2.5+}$ ”-like component.<sup>39</sup> Therefore, a room-temperature Mössbauer spectrum of  $\text{Fe}_3\text{O}_4$  will contain only two components: one originating from the  $A$  site  $\text{Fe}^{3+}$  ions, and the other from the  $B$  site  $\text{Fe}^{2.5+}$  ions. Each component is split into a sextet, due to hyperfine interactions between the nuclear magnetic dipole moment and the internal magnetic field caused by the ferrimagnetically ordered electron spins.

Upon oxidation, magnetite becomes nonstoichiometric, i.e., cation vacancies are created on the  $B$  sites.<sup>10</sup> They have a drastic influence on the electron hopping. Since every vacancy acts like an impurity with a minus 2.5 charge, five  $\text{Fe}^{3+}$  ions become trapped on surrounding octahedral sites, to screen its charge.<sup>40</sup> These ions are isolated from the hopping process. In the Mössbauer spectrum, their intensity  $I$  contributes to the component of the  $\text{Fe}^{3+}$  ions on the tetrahedral sites, since without an external magnetic field the hyperfine field  $B$  and isomer shift  $IS$  of octahedral and tetrahedral  $\text{Fe}^{3+}$  ions are nearly indistinguishable. So, the net effect is an intensity transfer from the  $\text{Fe}^{2.5+}$  component to the  $\text{Fe}^{3+}$  component. Therefore, the intensity ratio  $\beta = I(3+)/I(2.5+)$  of these two components is a very sensitive measure of the stoichiometry.<sup>10</sup> It is equal to 1/2 for stoichiometric  $\text{Fe}_3\text{O}_4$ , and goes to infinity for  $\gamma\text{-Fe}_2\text{O}_3$ .

The value of  $\delta$  can be calculated from  $\beta$  in the following way. Considering charge neutrality, we can write nonstoichiometric  $\text{Fe}_{3-\delta}\text{O}_4$  as  $\text{Fe}_A^{3+}[\text{Fe}_{1+2\delta}^{3+}\text{Fe}_{1-3\delta}^{2+}\square]_B\text{O}_4^{2-}$ , where  $\square$  stands for a vacancy. This leads to

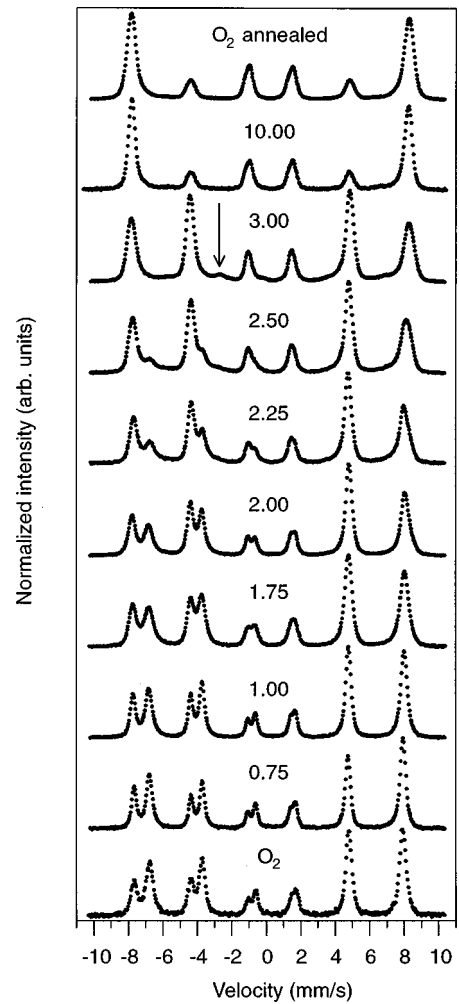


FIG. 2. Room temperature CEMS spectra of epitaxial  $\text{Fe}_{3-\delta}\text{O}_4/\text{MgO}(100)$  films, grown with  $\text{NO}_2$  as the oxidizing agent, as a function of the buffer volume pressure  $P_{buf}$ . This pressure (in mTorr) is indicated above each spectrum. For comparison, also a sample grown with 10 mTorr  $\text{O}_2$  (bottom spectrum) and a sample which has been annealed for 2 days in 1 atm  $\text{O}_2$  at 573 K (top spectrum) have been included.

$\text{Fe}_A^{3+}[\text{Fe}_{1-3\delta}^{3+}\text{Fe}_{1-3\delta}^{2+}\text{Fe}_{5\delta}^{3+}\square]_B\text{O}_4^{2-}$ , since every vacancy traps five  $\text{Fe}^{3+}$  ions. Including hopping, we finally obtain  $\text{Fe}_A^{3+}[\text{Fe}_{2-6\delta}^{2.5+}\text{Fe}_{5\delta}^{3+}\square]_B\text{O}_4^{2-}$ . So,  $\beta$  is given by

$$\beta = \frac{1 + 5\delta}{2 - 6\delta},$$

which leads to

$$\delta = \frac{2\beta - 1}{6\beta + 5}.$$

In principle, one should make a correction for the difference in the recoil-free fractions  $f$  of the  $A$  and  $B$  sites. However, it is not clear if there is any difference at all. Whereas Sawatzky *et al.* reported a ratio  $f_B/f_A = 0.94$ ,<sup>41</sup> later studies indicated that the recoil-free fractions are virtually identical.<sup>42</sup> In our analysis, we have assumed a ratio of 1.

In Fig. 2, a selection of room-temperature CEMS spectra is shown, measured with the gas detector setup, as a function of  $P_{buf}$ . For comparison, spectra of the 10.00 mTorr  $\text{O}_2$  and the  $\text{O}_2$ -annealed samples are also included. To find the value

of  $\beta$ , and therewith  $\delta$ , the spectra were fitted with two sextet components. To start with the spectrum of the 10.00 mTorr O<sub>2</sub> sample, this yielded an  $IS$  value (relative to  $\alpha$ -Fe) of 0.279(4) mm/s and  $B=48.69(3)$  for the first sextet, and  $IS=0.643(3)$  and  $B=45.47(2)$  for the second. The error bars in these values, i.e., the digits between brackets, are of statistical nature. Our fit parameters are in good agreement with literature reports for epitaxial Fe<sub>3</sub>O<sub>4</sub>/MgO(100) thin films.<sup>14,15,30,43</sup> The component with the larger  $B$  and smaller  $IS$  corresponds to the Fe<sup>3+</sup> component. An attempt to include a quadrupole splitting in the fits was made, but this did not decrease the error sum very much, nor did it yield significant values. In principle, a quadrupole splitting is expected, because the octahedral ions have trigonal instead of cubic site symmetry,<sup>42</sup> and because the film has an overall tetragonal distortion due to the lattice mismatch with the substrate. However, earlier reports also indicated that this splitting is negligible.<sup>43</sup> From the areas under the sextets, we find  $\beta=0.56(1)$ , which gives  $\delta=0.014(3)$ . Therefore, this sample is near-stoichiometric magnetite Fe<sub>3</sub>O<sub>4</sub>.

For low- $P_{buf}$  values (0.75-1.50 mTorr), the spectra are very similar to that of the 10.00 mTorr O<sub>2</sub> sample. However, for higher NO<sub>2</sub> fluxes, the Fe<sup>3+</sup> component starts to increase, at the expense of the Fe<sup>2.5+</sup> component. This indicates the formation of nonstoichiometric Fe<sub>3- $\delta$</sub> O<sub>4</sub>. At 2.75 mTorr, the Fe<sup>2.5+</sup> component has nearly vanished. For these high-flux spectra, the Fe<sup>3+</sup> intensity has to be fitted with two sextet components. This is because the  $IS$  and  $B$  of Fe<sup>3+</sup> ions on octahedral and tetrahedral sites are nearly, but not quite, the same.<sup>40</sup> Therefore, a one-Fe<sup>3+</sup>-component fit is an oversimplification for samples that are approaching  $\gamma$ -Fe<sub>2</sub>O<sub>3</sub>. Finally, at 10.00 mTorr NO<sub>2</sub>, only these two Fe<sup>3+</sup> components are left over, indicating the formation of stoichiometric  $\gamma$ -Fe<sub>2</sub>O<sub>3</sub>. This is supported by the fact that the spectrum is nearly identical to that of the O<sub>2</sub>-annealed film.

Interestingly, in the spectra of the 2.75–5.00 mTorr samples, there is a new component visible besides the dominant Fe<sup>3+</sup> contribution. This small component, with an estimated hyperfine field of  $\sim 40$  T, can best be seen between the second and third peak from the left, as indicated by the arrow in Fig. 2. Unfortunately, it was not possible to fit it satisfactorily, not even with a quadrupole splitting. Probably, this component can only be resolved by applying an external field. To estimate a value of  $\beta$  for these spectra, the residual intensity was integrated and attributed to Fe<sup>2.5+</sup> ions. However, we point out that this might not be valid, which makes the results of our analysis for this kind of sample uncertain. For example, if the electron hopping has completely ceased, the component could also be due to isolated Fe<sup>2+</sup> ions, similar to spectra of Fe<sub>3</sub>O<sub>4</sub> below the Verweij transition.<sup>14,43</sup> However, the ultimate disappearance of all Fe<sup>2.5+</sup> and Fe<sup>2+</sup> components at  $P_{buf}=10.00$  mTorr, combined with the change in the thin film magnetization direction (see Sec. III B), enables an easy distinction between stoichiometric  $\gamma$ -Fe<sub>2</sub>O<sub>3</sub> and near-stoichiometric specimens (e.g., Fe<sub>3- $\delta$</sub> O<sub>4</sub> with  $\delta\sim 0.3$ ). This cannot be done with the same degree of certainty if conventional techniques, such as XPS,<sup>44</sup> are used. Furthermore, XPS is only a surface-sensitive technique, whereas CEMS probes the entire film.

In Fig. 3, the value of  $\delta$  as a function of  $P_{buf}$  is plotted.

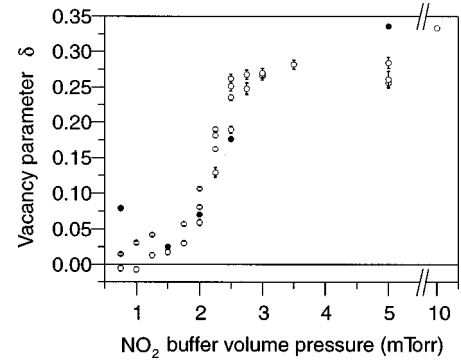


FIG. 3. The number of vacancies  $\delta$  per formula unit Fe<sub>3- $\delta$</sub> O<sub>4</sub>, as a function of the buffer volume pressure  $P_{buf}$ . Open circles: values derived from fits to the CEMS spectra (Fig. 2). Filled circles: results from magneto-optical Kerr spectroscopy (Ref. 13).

Of 5 samples, the stoichiometry has also been determined by MOKE spectroscopy.<sup>13</sup> For comparison, these data points are included in the graph. They agree well with the CEMS data. From the figure, we can conclude that with NO<sub>2</sub> as the oxidizing agent, it is possible to prepare all magnetite phases, i.e., not only stoichiometric Fe<sub>3</sub>O<sub>4</sub> and  $\gamma$ -Fe<sub>2</sub>O<sub>3</sub>, but also all intermediate nonstoichiometric Fe<sub>3- $\delta$</sub> O<sub>4</sub> phases. As mentioned earlier, with O<sub>2</sub>, only Fe<sub>3</sub>O<sub>4</sub> and Fe<sub>3- $\delta$</sub> O<sub>4</sub> with  $\delta\leq 0.06$  could be prepared.<sup>15</sup> Therefore, these data prove that NO<sub>2</sub> is a much more efficient oxidizing agent, equivalent to oxygen plasma.<sup>21</sup> From the geometry of the MBE setup, it can be calculated that the oxidation process is largely kinetically controlled, i.e., the  $P_{buf}$  values needed to induce stoichiometric Fe<sub>3</sub>O<sub>4</sub> correspond to a regime where the ratio of NO<sub>2</sub> and Fe fluxes at the substrate surface is  $\sim 4/3$ .

### B. Zero-field magnetization directions

One intriguing aspect of the CEMS spectra is the variation in the relative intensities of the 6 lines in the sextets. Theoretically, they relate as 3: $x$ :1:1: $x$ :3, where  $x$  depends on the angle  $\theta$  between the incident  $\gamma$ -rays and the direction of the magnetic hyperfine field  $\mathbf{B}$ ,<sup>46</sup> i.e.,  $x=4\sin^2\theta/(1+\cos^2\theta)$ . Therefore, the relative intensities directly reveal the average direction of the magnetization in the thin film: a value of  $x=0$  corresponds to a perpendicular magnetization direction ( $\theta=0^\circ$ ), and  $x=4$  indicates an in-plane direction ( $\theta=90^\circ$ ). In Fig. 4, we have plotted  $x$  as a function of the stoichiometry, i.e., the value of  $\delta$ . For the low-flux samples, up to and including 2.50 mTorr, the value of  $x$  is an average of the Fe<sup>3+</sup> and Fe<sup>2.5+</sup> components; for the higher-flux samples, only the Fe<sup>3+</sup> component is taken into account.

For near-stoichiometric Fe<sub>3</sub>O<sub>4</sub> films,  $x$  is close to 2, in agreement with results of Fujii *et al.*<sup>14,15,30,43</sup> A value of 2 indicates either a random direction of the magnetization, or a magnetization parallel to the  $\langle 111 \rangle$  directions. At room temperature, the 4 equivalent  $\langle 111 \rangle$  directions are the magnetic easy axes in bulk Fe<sub>3</sub>O<sub>4</sub>. They all make angles of 54.74° with the [001] film normal, i.e., the direction of incidence of the  $\gamma$  rays. Therefore,  $x$  will be 2, for all magnetic domains.<sup>14</sup> At first sight, this seems to be a logical explanation, however, a closer examination shows that it is not. In the case of thin films, the shape anisotropy is an order of magnitude larger than the crystal and magnetoelastic anisotropy terms,

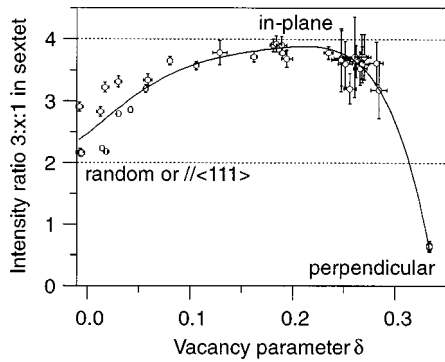


FIG. 4. Variation of the intensity ratio 3: $x$ :1:1: $x$ :3 of the sextet components in the CEMS spectra (Fig. 2), as a function of the stoichiometry, i.e., the number of vacancies  $\delta$  per formula unit  $\text{Fe}_{3-\delta}\text{O}_4$  (Fig. 3). Plotted is the value of  $x$ , the relative intensities of the second and fifth lines. The solid line is a guide for the eye.

and therefore, the magnetization should lie entirely in-plane ( $x=4$ ).<sup>6,38</sup> As the magnetite is oxidized to  $\text{Fe}_{3-\delta}\text{O}_4$ , the spins indeed turn towards the film plane, although never completely. Anomalous out-of-plane components have also been reported by Margulies *et al.*<sup>38</sup> However, a direct comparison with their measurements is not possible, because of differences in sample preparation. Especially, we point out to the very high substrate temperature of 773 K used in their experiments, which must have led to extensive interdiffusion at the  $\text{MgO}/\text{Fe}_3\text{O}_4$  interface (see Secs. III C and III D). For example, whereas the films of Margulies *et al.* could not be saturated in magnetic fields even as high as 7 T,<sup>38</sup> pure  $\text{Fe}_3\text{O}_4$  films prepared by our method or with  $\text{O}_2$ -assisted MBE are easily saturated in fields of  $\sim 0.5$  T.<sup>6,7,13</sup>

Considering the dominant shape anisotropy for thin films, it is remarkable that for stoichiometric  $\gamma\text{-Fe}_2\text{O}_3$ , the magnetization becomes almost perpendicular to the film plane. Such a perpendicular magnetization direction has been found before in  $\text{CoO}/\text{Co}_x\text{Fe}_{3-x}\text{O}_4$  and  $\text{CoO}/\text{Fe}_3\text{O}_4$  bilayers,<sup>45</sup> but

never in single  $\text{Fe}_3\text{O}_4$  films. Apparently, the shape anisotropy is overruled by an even more dominant anisotropy term, but at present, we do not know its nature. It is also very interesting that for (near-)stoichiometric  $\text{Fe}_3\text{O}_4$ ,  $x$  is always significantly larger for the  $\text{Fe}^{2.5+}$  component than for the  $\text{Fe}^{3+}$  component. In stoichiometric  $\text{Fe}_3\text{O}_4$ , the  $\text{Fe}^{2.5+}$  and  $\text{Fe}^{3+}$  components directly correspond to octahedral and tetrahedral sites, respectively. Therefore, this result implies that in these thin films, the two cation sublattices are not coupled completely antiparallel, in contrast to bulk crystals. On average, the magnetization of the  $B$  site ions is  $4^\circ$  closer to the film plane than the magnetization of the  $A$  site ions. This is difficult to understand, because the  $A$ -site  $\text{Fe}^{3+}$  ions, with  $3d^5$  configuration, are supposed to have no orbital angular momentum that could couple with the lattice.

### C. Surface reconstructions

When magnetite films are deposited on  $\text{MgO}(100)$ , the RHEED and LEED patterns differ from those expected for a bulk-terminated surface. Figure 5 shows RHEED patterns of (a) a clean  $\text{MgO}(100)$  substrate, and (b) an  $\text{Fe}_3\text{O}_4(100)$  film. Because the growth is fully coherent, the in-plane dimensions of the spinel unit cell of  $\text{Fe}_3\text{O}_4$  are exactly twice those of the rocksalt unit cell of  $\text{MgO}$ . Therefore, one expects a set of diffraction rods with half the spacing of the substrate, i.e., the number of lines in the pattern will double. When we study the evolution of the RHEED pattern as a function of deposition time, we indeed observe the development of these extra, half order diffraction rods in the zeroth Laue zone. This happens after the formation of approximately 1 ML. When the deposition process is continued, however, a new set of diffraction rods appears upon formation of the second ML. These rods are positioned exactly in between the half-order rods. This can only be seen when the beam is incident along a  $[100]$  direction. With the beam incident along  $[110]$ , the extra quarter-order rods do not show up. These observa-

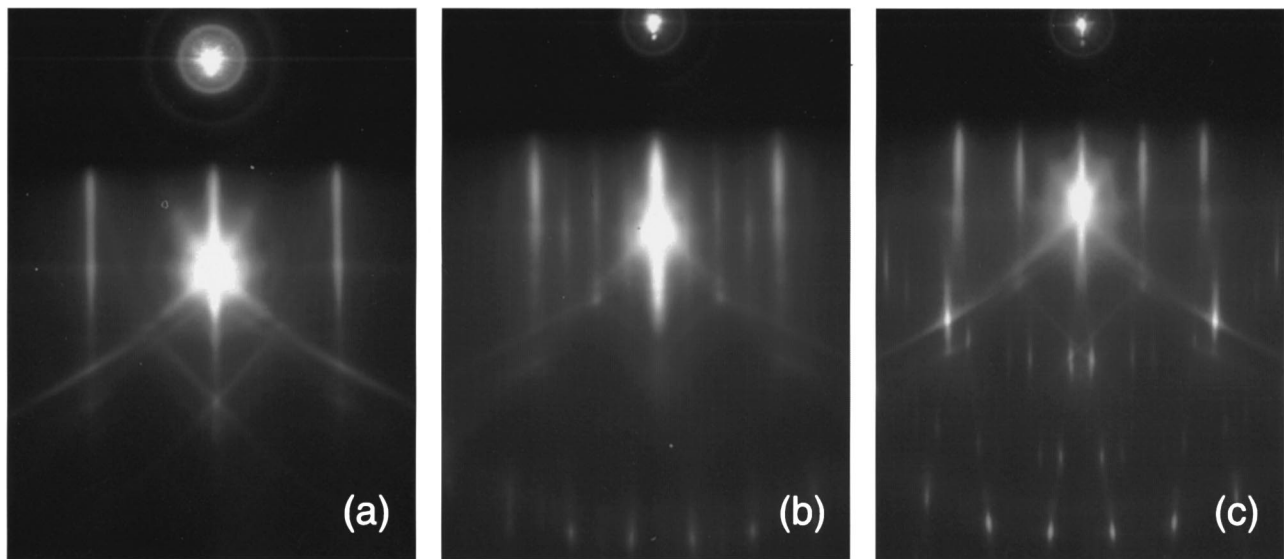


FIG. 5. RHEED patterns, recorded at an electron energy of 15 keV with the beam incident along a  $[100]$  direction. (a) An *ex situ* cleaved and UHV-annealed  $\text{MgO}(100)$  substrate. (b) An epitaxial  $\text{Fe}_{3-\delta}\text{O}_4(100)$  film with a  $(\sqrt{2} \times \sqrt{2})\text{R}45^\circ$  reconstruction. This pattern is independent of the value of  $\delta$ , i.e., it is also observed for the stoichiometric magnetite  $\gamma\text{-Fe}_2\text{O}_3$  phase. (c) A  $3 \times 1$  reconstructed  $\text{Fe}_3\text{O}_4/\text{MgO}(100)$  film.

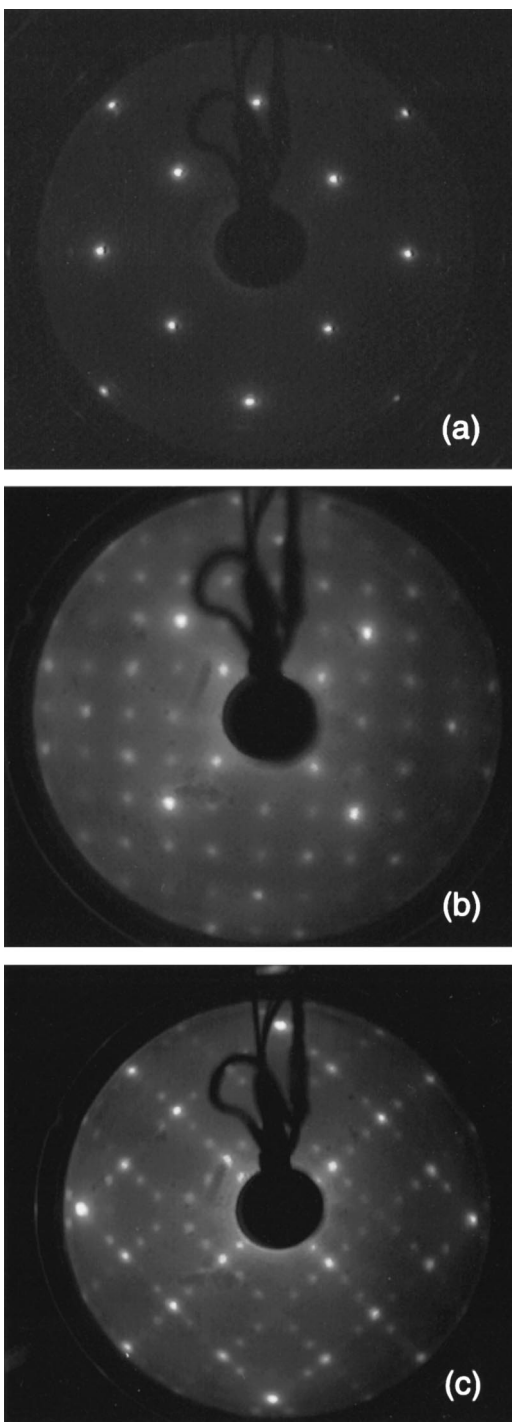


FIG. 6. LEED patterns, corresponding to the RHEED patterns displayed in Fig. 5: (a) an *ex situ* cleaved and annealed MgO(100) substrate, (b) a  $(\sqrt{2} \times \sqrt{2})R45^\circ$  reconstructed Fe<sub>3</sub>O<sub>4</sub>/MgO(100) surface, and (c) a  $3 \times 1$  reconstructed Fe<sub>3</sub>O<sub>4</sub>/MgO(100) surface. The patterns were recorded at electron beam energies of 119, 106, and 156 eV, respectively.

tions are also confirmed by LEED; see Fig. 6. Along the  $\langle 110 \rangle$  directions, the number of spots merely doubles, whereas along the  $\langle 100 \rangle$  directions, it becomes fourfold.

The LEED diffraction spots of the Fe<sub>3</sub>O<sub>4</sub> film form a square mesh, that is rotated over  $45^\circ$  with respect to the MgO pattern. Its dimensions relative to those of the MgO mesh are  $\frac{1}{4}\sqrt{2}:1$ . Therefore, the observed patterns correspond

to a  $(\sqrt{2} \times \sqrt{2})R45^\circ$  reconstruction with respect to the smallest unit cell of a bulk-terminated Fe<sub>3</sub>O<sub>4</sub> (100) surface. Confusingly, this reconstruction was originally labeled as  $p(1 \times 1)$  by Tarrach *et al.*,<sup>47</sup> indicating that it constituted a symmetry change from face-centered cubic to primitive cubic at the surface. However, this is not a valid label within the conventional framework of the Wood's notation.

The  $(\sqrt{2} \times \sqrt{2})R45^\circ$  reconstruction was first observed on natural single crystals, after Ar<sup>+</sup> sputtering and annealing, by Tarrach *et al.*<sup>47</sup> and subsequently on MBE-grown epitaxial Fe<sub>3</sub>O<sub>4</sub> films by Voogt *et al.*,<sup>48</sup> being later confirmed by other MBE growth studies.<sup>18,27,37,45</sup> In two earlier thin film growth studies, only  $1 \times 1$  RHEED patterns had been observed, corresponding to unreconstructed surfaces.<sup>21,49</sup> An examination of these studies shows that the reconstruction is independent of the oxidizing agent, i.e., it is observed irrespective of the use of NO<sub>2</sub>, molecular O<sub>2</sub>, or oxygen plasma. As a matter of fact, the  $(\sqrt{2} \times \sqrt{2})R45^\circ$  reconstruction of the Fe<sub>3</sub>O<sub>4</sub>(100) surface is very universal. We observe it not only afterwards under UHV conditions, but also during deposition of the films, at all substrate temperatures above 273 K. It is independent of the stoichiometry; all our Fe<sub>3</sub>O<sub>4</sub>,  $\gamma$ -Fe<sub>2</sub>O<sub>3</sub>, and intermediate Fe<sub>3- $\delta$ O<sub>4</sub> samples exhibit it. This indicates that the  $(\sqrt{2} \times \sqrt{2})R45^\circ$  reconstruction is an intrinsic property of the (100) surfaces.</sub>

So far, this reconstruction has only been interpreted in terms of an electron counting model.<sup>18,37,47</sup> However, the driving force can also be understood from simple electrostatic considerations, as demonstrated by Barbieri *et al.* for the Fe<sub>3</sub>O<sub>4</sub>(111) surface.<sup>50</sup> According to Tasker,<sup>51</sup> a surface of an ionic or partly ionic crystal falls into one of three categories. The first, type 1, has atomic planes parallel to the surface that contain both anions and cations. The net charge per plane is zero. Examples are the (100) and (110) planes of rocksalt oxides, such as MgO, NiO, etc. The type-2 surface has charged planes parallel to the surface, but the stacking is in such a symmetric way that the repeat unit does not have a dipole moment perpendicular to the surface. An example is the *c* or (001) plane in the corundum structure of  $\alpha$ -Al<sub>2</sub>O<sub>3</sub> and  $\alpha$ -Fe<sub>2</sub>O<sub>3</sub>. The last surface, type 3, also has charged planes. However, the stacking sequence lacks the symmetry of the type-2 surface, and the result is a dipole moment in the repeat unit, perpendicular to the surface. Examples are the (111) surfaces in the rocksalt structure. These surfaces are called polar. The consequence of a dipole moment perpendicular to the surface is that the surface energy diverges. Therefore, such polar surfaces cannot exist as simple bulk terminations: they have to be stabilized by reconstructions and/or adsorption of (charged) foreign species.

When viewed along the [001] axis, the Fe<sub>3</sub>O<sub>4</sub>(100) surface consists of an alternating stack of planes containing only tetrahedral Fe<sup>3+</sup> cations, and planes containing both O<sup>2-</sup> anions and octahedral Fe<sup>2.5+</sup> cations. The charges in these A and B planes per unit cell are +6 and -6, respectively. Thus, the Fe<sub>3</sub>O<sub>4</sub>(100) surface is a polar type-3 one, and *has therefore to reconstruct*. Note that the polarity of the Fe<sub>3- $\delta$ O<sub>4</sub>(100) surface does not depend on the stoichiometry; all phases are equally polar. The charge per unit cell in a B layer is given by  $8O^{2-} + (4 - 2\delta) \times Fe^{2.5+} + 10\delta \times Fe^{3+}$ ; this is a constant value of -6, as in stoichiometric Fe<sub>3</sub>O<sub>4</sub>. There-</sub>

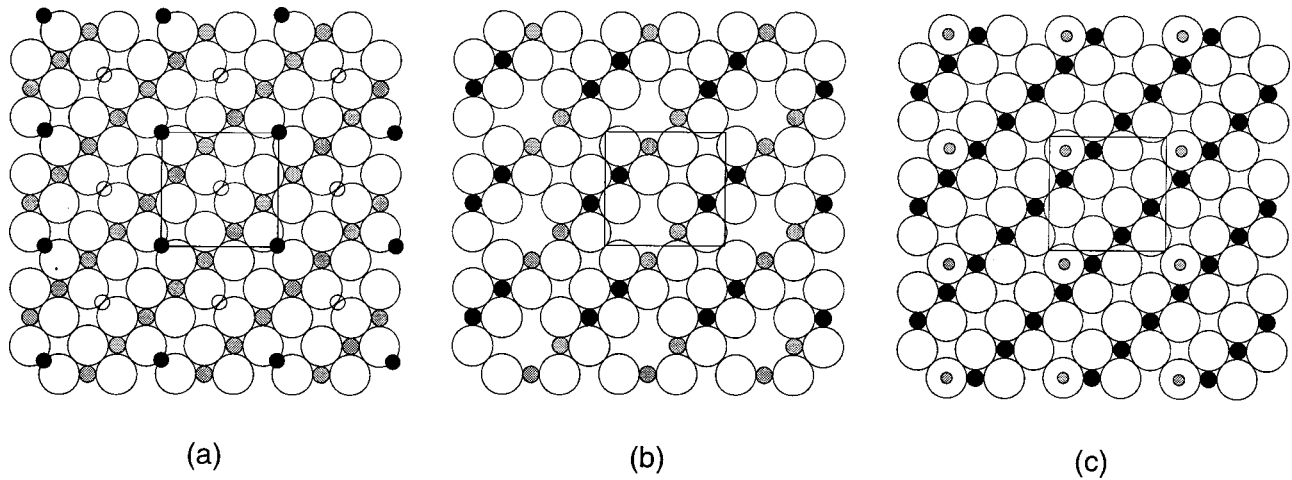


FIG. 7. Three possible surface structures for the  $(\sqrt{2} \times \sqrt{2})R45^\circ$  reconstructed  $\text{Fe}_3\text{O}_4(100)$  surface, in top view. (a) A termination at a half-filled  $A$  layer of  $\text{Fe}^{3+}$  ions. (b) A termination at a  $B$  layer of oxygen anions and octahedral  $\text{Fe}^{2.5+}$  ions. There is one oxygen vacancy per unit cell, accompanied by the oxidation of two  $\text{Fe}^{2.5+}$  ions to  $\text{Fe}^{3+}$ . The remaining  $\text{Fe}^{2.5+}$  ions are trapped by the oxygen vacancies, resulting in charge ordering. (c) An alternative termination at a  $B$  layer. Here, the surface does not contain oxygen vacancies, but one hydroxyl group per unit cell. Furthermore, the surface is fully oxidized, containing only  $\text{Fe}^{3+}$  ions. Large open circles: oxygen anions; small open circles: missing  $\text{Fe}^{3+}$  ions; black filled circles:  $\text{Fe}^{3+}$  ions; large gray filled circles:  $\text{Fe}^{2.5+}$  ions; small gray filled circles: hydrogen. In each case, the bulk unit cell is outlined.

fore, a reconstruction is expected for all magnetite phases, including  $\gamma\text{-Fe}_2\text{O}_3$ .

At this point, we want to address a recent controversial issue. Namely, our results are at odds with those reported by Chambers and co-workers. Using oxygen plasma-assisted MBE, they find that the (100) surface of  $\gamma\text{-Fe}_2\text{O}_3$  is not reconstructed.<sup>44</sup> Most likely, the opposite nature of this observation is a reflection of the different preparation conditions used. To explain their results, Chambers *et al.* assume a termination at a full  $A$  layer, with one octahedral Fe vacancy per unit cell in the  $B$  layer below. Using the electron counting approach, they claim that this is an autocompensated, stable surface. However, we have reason to believe that their analysis is wrong. In the bulk  $\gamma\text{-Fe}_2\text{O}_3$  structure, each  $B$  layer has two thirds of an Fe vacancy per unit cell, compared to  $\text{Fe}_3\text{O}_4$ . In their analysis, Chambers *et al.* correctly assign half of an electron from a  $B$  site Fe ion to an octahedral covalent bond (in the  $\text{Fe}_3\text{O}_4$  structure, the Fe ions donate only 5/12 electrons). By doing so, the vacancies in the bulk are implicitly taken into account. In the structural model under question, the surface  $B$  layer has 1 vacancy, i.e., one-third more than in the bulk. The point is that only this extra one-third of a vacancy should be considered, not the entire vacancy. Then, the analysis yields a nonautocompensated, unstable surface. The same conclusion can be drawn by applying the electrostatic approach: in the proposed structure, the charges per unit cell in the surface and subsurface layers are +6 and -7, respectively, therewith creating an even more polar surface. Note that a discrepancy in the outcome of the two approaches is impossible, as Pashley has demonstrated that the electron counting and electrostatic models are equivalent.<sup>52</sup> Similarly, it has also been suggested that an auto-compensated  $\text{Fe}_{1-x}\text{O}$  layer might form the surface of  $\text{Fe}_3\text{O}_4$ .<sup>37</sup> However, such a wustite layer, with zero charge, cannot eliminate the polarity of the surface either.

Coming back to the electrostatic model, type-3 surfaces can be stabilized by reducing the charge in the surface plane

to one half. This transforms the type-3 surface into a type-2 one, with a new three-plane repeat unit with no dipole moment. Such a reconstruction does not include contamination. So far, the  $(\sqrt{2} \times \sqrt{2})R45^\circ$  reconstruction has only been explained with a termination at a half-filled  $A$  layer,<sup>18,27,37</sup> as suggested originally by Tarrach *et al.*<sup>47</sup> Here, every second  $\text{Fe}^{3+}$  ion has been removed in a regular way; see Fig. 7(a). Such a layer has a charge of +3 per unit cell instead of +6, thereby making a stable surface. However, our point is that the surface might equally well be terminated at a  $B$  layer. In this case, the charge per unit cell could be reduced from -6 to -3 by, for example, creating one  $\text{O}^{2-}$  vacancy and oxidizing two  $\text{Fe}^{2.5+}$  ions to  $\text{Fe}^{3+}$ , see Fig. 7(b). There are many variations on this theme, for example, the creation of two oxygen vacancies, accompanied by the reduction of two  $\text{Fe}^{2.5+}$  ions to  $\text{Fe}^{2+}$ , or the creation of 3 oxygen vacancies per two unit cells without Fe valency change, have the same effect. Such a  $B$  layer, with a constant stoichiometry, could be present on all  $\text{Fe}_{3-\delta}\text{O}_4$  films, irrespective of the stoichiometry of the interior. In fact, probe layer Mössbauer spectroscopy has suggested a surface termination at a  $B$  layer, with a higher  $\text{Fe}^{3+}$  content than in the bulk.<sup>30</sup>

This kind of surface might have interesting consequences. To speculate, an ordered array of oxygen vacancies in a  $B$  layer could induce an ordering of the charges on the neighboring Fe ions. As discussed above, an Fe vacancy on an octahedral site acts like an impurity with a charge of minus 2.5, and repels conduction electrons from neighboring sites.<sup>40</sup> Similarly, an oxygen vacancy acts like a 2+ impurity, and could trap conduction electrons on neighboring cation  $B$  sites. This has been illustrated in Fig. 7(b), for the case of one vacancy per unit cell. Here, we assumed that the  $\text{Fe}^{2.5+}$  ions are trapped at the oxygen vacancy sites. The resulting charge ordering looks very similar to that observed with spin-sensitive STM on natural single crystals.<sup>53</sup>

As a third possibility, we mention the case of a  $B$  surface layer that does not contain oxygen vacancies, but hydroxyl

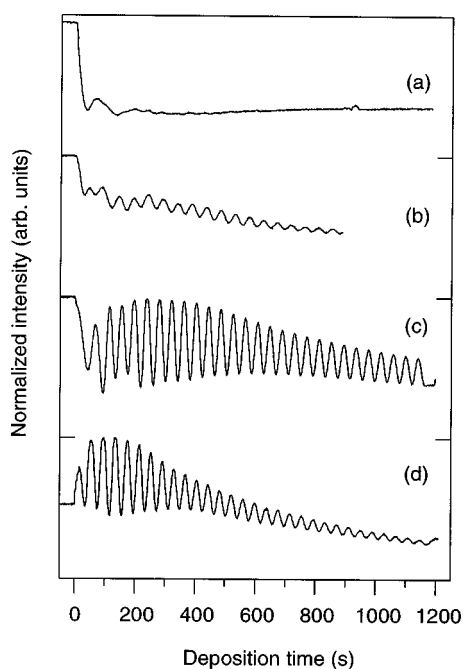


FIG. 8. RHEED intensity oscillations of the specularly reflected electron beam, observed during deposition of Fe<sub>3</sub>O<sub>4</sub> on (a) polished and annealed MgO(100), (b) *in situ* cleaved MgO(100), (c) *ex situ* cleaved and annealed MgO(100), and (d) an annealed Fe<sub>3</sub>O<sub>4</sub>/MgO(100) film. In each case, the electron beam was incident along a [100] direction, with a primary energy of 15 keV, at an angle of 0.68° corresponding to the first anti-Bragg position of Fe<sub>3</sub>O<sub>4</sub>.

groups. With XPS, the presence of hydrogen can only be inferred indirectly, namely if it is present as hydroxyl, OH<sup>1-</sup>, groups. Then, a second O 1s peak will appear, shifted by ~1.5 eV to the higher binding-energy side.<sup>54</sup> Such a peak was not observed.<sup>51</sup> If, however, the hydrogen fraction is relatively small, it will only cause an asymmetry in the peak shape of the main O 1s line. Considering the resolution of our XPS instrument, i.e., ~1.0 eV, we cannot fully exclude or confirm the presence of hydroxyl groups. One possibility is a fully oxidized *B* layer, in which one O<sup>2-</sup> ion per unit cell has been replaced by an OH<sup>1-</sup> group, i.e., a composition of Fe<sub>4</sub><sup>3+</sup>O<sub>7</sub><sup>2-</sup>OH<sup>1-</sup> per unit cell. This is shown in Fig. 7(c). Such a layer has a charge of -3 per unit cell, thus also creating a nonpolar, stable surface.

Interestingly, a termination at a *B* layer, either with vacancies or hydroxyl groups, would invalidate all previous interpretations of STM images of the ( $\sqrt{2} \times \sqrt{2}$ )R45° reconstructed Fe<sub>3</sub>O<sub>4</sub>(100) surface.<sup>37,47,55</sup> These STM images revealed objects in a ( $\sqrt{2} \times \sqrt{2}$ )R45° lattice, which were slightly protruded above the surface. In all of these studies, it was claimed that only Fe atoms were imaged. Therefore, it is tempting to ascribe these objects to Fe<sup>3+</sup> ions, corresponding with a surface terminated at a half-filled *A* layer. However, these objects have so far not been identified satisfactorily. Furthermore, they changed their appearance with the sample bias voltage. Only recently, Gaines *et al.* have been able to resolve the objects into two single, spherical features.<sup>55</sup> These were ascribed to pairs of tetrahedral Fe<sup>3+</sup> ions, i.e., a distorted, but full *A* layer. This is in contradiction with both the electrostatic and the electron counting models. However,

it is questionable if these STM images represent an as-grown ( $\sqrt{2} \times \sqrt{2}$ )R45° Fe<sub>3</sub>O<sub>4</sub>(100) surface, because of the sputtering and annealing treatments that were needed to clean the *ex situ* grown samples. Furthermore, it should be kept in mind that with STM one does not observe atoms, but merely a density of states (empty or filled). Therefore, the unidentified objects in a ( $\sqrt{2} \times \sqrt{2}$ )R45° lattice might be surface states that are associated with hydroxyl groups, oxygen vacancies and/or ordered Fe charges. As a matter of fact, the claim that only Fe atoms can be imaged with STM, has recently been contradicted by studies of an FeO monolayer on Pt(111).<sup>56</sup>

The ( $\sqrt{2} \times \sqrt{2}$ )R45° reconstruction is very persistent. Only after prolonged annealing at high temperatures does it disappear. Figure 6(c) shows a LEED pattern of a 5.0 nm-thick Fe<sub>3</sub>O<sub>4</sub>(100) film, that has been annealed for 1 h at 875 K in an O<sub>2</sub> pressure of 1 × 10<sup>-4</sup> Pa. The pattern corresponds in essence to unreconstructed 1 × 1 Fe<sub>3</sub>O<sub>4</sub>. However, the number of diffraction spots has tripled along the ⟨110⟩ directions, indicating a 3 × 1 reconstruction, with respect to the bulk spinel unit cell. The reconstruction consists of two domains; the long axis of the surface unit cell is either in the [110] or in the [1 $\bar{1}$ 0] direction. The absence of extra diffraction spots in other directions eliminates the possibility of a 3 × 3 reconstruction. This is confirmed by the RHEED pattern from this sample [Fig. 5(c)]. We find that the change from ( $\sqrt{2} \times \sqrt{2}$ )R45° to 3 × 1 is irreversible; further annealing, either in vacuum or in O<sub>2</sub>, cannot restore the ( $\sqrt{2} \times \sqrt{2}$ )R45° or 1 × 1 patterns.

XPS core level spectra (not shown) of the Fe 2*p* edge after annealing indicate the formation of an oxide, containing mostly Fe<sup>3+</sup> ions. The spectra are similar to those of the α-Fe<sub>2</sub>O<sub>3</sub> and γ-Fe<sub>2</sub>O<sub>3</sub> phases, with a binding energy of the main peak of 710.9 eV, and a strong Fe<sup>3+</sup> satellite at 719 eV.<sup>24,31</sup> Furthermore, the signal from the Mg *KLL* Auger edge strongly increases with annealing. This indicates extensive compound formation at the MgO/Fe<sub>3</sub>O<sub>4</sub> interface. Studies have indicated that the onset of interdiffusion is at temperatures around ~625–675 K.<sup>27</sup> Therefore, it is most likely that the entire Fe<sub>3</sub>O<sub>4</sub> film has been converted into Mg ferrite, MgFe<sub>2</sub>O<sub>4</sub>.

Apparently, some Mg ions diffuse all the way through the film to the surface. Having reached the surface, they form structures parallel or normal to the rows of *B* site cations. To explain the threefold superstructure, it must be assumed that only every third row is decorated, i.e., rows that are 1.8 nm apart. Recently, such a structure has indeed been observed with STM.<sup>55</sup> Then, the two-domain structure in the reconstruction originates from a rotation of the octahedral *B* site cations over 90°. This rotation occurs when going up or down between terraces that are separated by a step with a height of 2*n* + 1 monolayers, or when there are stacking faults in the film.<sup>7,8,37</sup>

The 3 × 1 reconstruction has also been observed by Gaines *et al.*<sup>55</sup> Furthermore, Anderson *et al.* reported a very akin 4 × 1, which was also induced by Mg segregation.<sup>27</sup> It is not clear what causes the division into three- and fourfold reconstructions. Anderson *et al.* used much thicker films (~1 μm), which probably led to structures less rich in Mg at the surface.

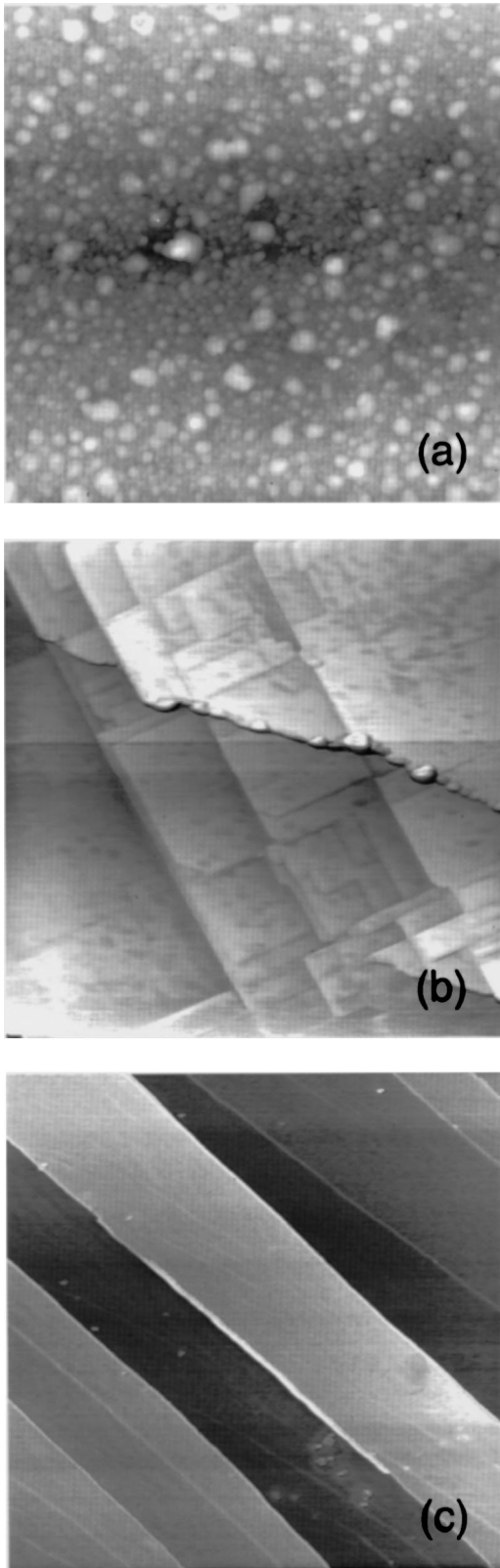


FIG. 9. AFM images of various MgO(100) substrates corresponding to the RHEED oscillations displayed in Fig. 8(a)–8(c): (a) polished and annealed (scan size  $5 \times 5 \mu\text{m}^2$ ), (b) *in situ* cleaved ( $5 \times 5 \mu\text{m}^2$ ), and (c) *ex situ* cleaved and annealed ( $18 \times 18 \mu\text{m}^2$ ).

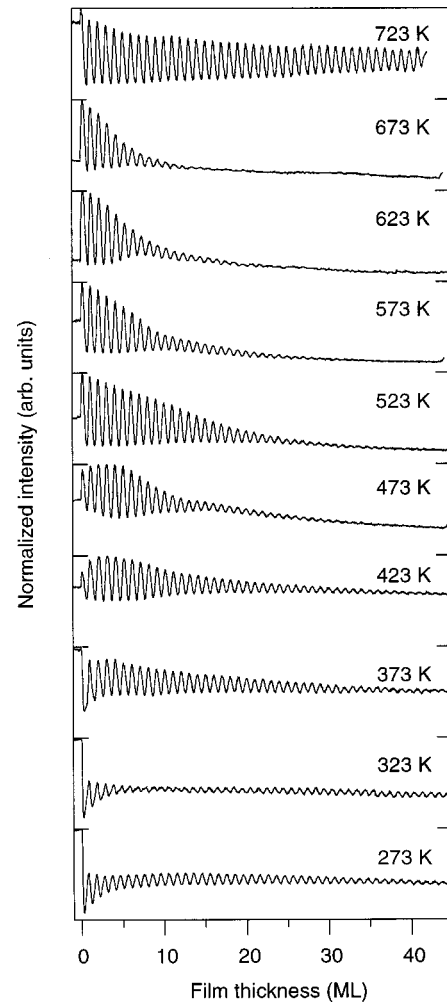


FIG. 10. RHEED intensity oscillations, observed during deposition of  $\text{Fe}_3\text{O}_4$  on annealed  $\text{Fe}_3\text{O}_4/\text{MgO}(100)$  films, as a function of the substrate temperature. The electron beam was incident along a  $[100]$  direction, in the first anti-Bragg position ( $0.68^\circ$ ), at an energy of 15 keV.

#### D. RHEED intensity oscillations

During deposition of the films, we observe oscillations in the intensity of the specularly reflected beam. Figure 8(c) displays a typical curve, measured during deposition on an *ex situ* cleaved and annealed MgO(100) substrate (with  $T_{\text{sub}} = 523$  K). These oscillations are indicative of a two-dimensional (2D) layer-by-layer, or Frank–van der Merwe, growth mode.<sup>57–59</sup> The period of the oscillations corresponds to the formation time of 1 ML. For  $\text{Fe}_3\text{O}_4$  to  $\gamma\text{-Fe}_2\text{O}_3$ , such a monolayer has a thickness of 0.21 nm, and consists of a (100)-oriented slab of oxygen anions, together with the appropriate amount of cations to maintain charge neutrality.

To study the influence of substrate preparation, we compared the *ex situ* cleaved and UHV-annealed substrates with commercially available polished MgO(100) [Fig. 8(a)], *in situ* cleaved MgO(100) [Fig. 8(b)], and an annealed  $\text{Fe}_3\text{O}_4/\text{MgO}(100)$  film [Fig. 8(d)]. The polished MgO was cleaned by annealing in an identical way as the *ex situ* cleaved substrate, the *in situ* cleaved MgO(100) surface was prepared by breaking a crystal inside the UHV system, without further heat treatment, and the  $\text{Fe}_3\text{O}_4(100)$  film was prepared by annealing for 1 h at 875 K in  $1 \times 10^{-6}$  Pa  $\text{O}_2$ . All

oscillation curves in Fig. 8 were recorded with the electron beam incident along a [100] direction, at an incidence angle of 0.68°, and an electron energy of 15 keV.

There are some clear differences between the four substrates: going from polished, via *in situ* cleaved, to the *ex situ* cleaved MgO(100), the number and amplitude of the oscillations both strongly increase. The annealed Fe<sub>3</sub>O<sub>4</sub>/MgO(100) film behaves similar to the *ex situ* cleaved MgO(100). This trend reflects the behavior that was observed earlier for NiO and CoO growth on MgO(100).<sup>23</sup>

At present, there is consensus that these oscillations reflect periodic changes in surface morphology, associated with 2D layer-by-layer growth.<sup>59</sup> In the simplest of pictures, they are caused by destructive interference of electrons, scattered from terraces that are separated by a step with a height of 1 ML. Thus, oscillations should only be observable when the angle of incidence  $\theta$  of the electron beam fulfills the anti-Bragg condition. However, it is well-known that oscillations can be observed for other values of  $\theta$  as well.<sup>60</sup> Combined STM and RHEED studies on GaAs homoepitaxy have indicated that also diffuse scattering at step edges should be taken into account.<sup>61</sup> In this model, the step-density, defined as the step-length per unit area, plays an important role. Again, this parameter oscillates during the formation of a new monolayer.

To study the origin of our RHEED oscillations in more detail, we examined the morphology of the substrates. Figure 9 shows atomic force microscopy (AFM) images of (a) polished and annealed MgO(100), (b) *ex situ* cleaved MgO(100), and (c) *ex situ* cleaved and annealed MgO(100). The images were measured in air, with a NanoScope-II AFM operated in contact mode. The *ex situ* cleaved MgO [Fig. 9(b)] exhibits large macrosteps, separating large terraces. These steps have heights of  $\sim 150$  nm, and run approximately normal to the direction of cleavage. On the large terraces, a second ‘‘patchwork’’ structure is visible, consisting of smaller steps. These steps run in the  $\langle 100 \rangle$  directions, and have average heights of  $\sim 2$  nm, i.e., a few unit cells of MgO. Upon annealing, the morphology changes markedly [Fig. 9(c)]. The macrosteps remain, but the small steps have disappeared. As a result, the surface now consists of broad, flat surfaces, with widths of  $\sim 1$   $\mu$ m. We point out that in both images, the resolution is not high enough to resolve atomic steps, with heights of only 0.21 nm or small multiples thereof. Nevertheless, the AFM images are in qualitative agreement with x-ray diffraction studies by Kim *et al.*<sup>62</sup> who show that annealing leads to a reduction in the number of minor steps, giving large, atomically flat terraces.

The *in situ* cleaved substrate is similar to the *ex situ* cleaved MgO(100) before annealing, having macrosteps of up to  $\sim 225$  nm and minor steps on the terraces of  $\sim 1.5$  nm. In contrast, the polished MgO has a very rough surface. Although this kind of substrate appears very flat, i.e., it has mirror-like surfaces for the naked eye (no macrosteps), the AFM image [Fig. 9(a)] shows terraces that are full of three-dimensional (3D) islands. In contrast, two STM studies on Fe<sub>3</sub>O<sub>4</sub>/MgO(100) films by other authors revealed a morphology consisting of very large (typical dimensions 10 to 100 nm), atomically flat surfaces.<sup>27,37</sup> Thus, these surfaces are comparable in smoothness to the *ex situ* cleaved and annealed MgO.

Considering these initial morphologies, the differences in the RHEED intensity oscillations can be interpreted in terms of step density. In the cases of smooth *ex situ* cleaved and annealed MgO and annealed Fe<sub>3</sub>O<sub>4</sub>/MgO films, the variation in the step density due to layer-by-layer growth will be relatively large, with respect to the mean step density. Hence, also the specular spot intensity will show large variations. In contrast, the polished MgO surface has a very high initial step-density, and the variations due to layer-by-layer growth will be relatively small with respect to the mean step density. Consequently, also the intensity oscillations will be hardly discernible. The *in situ* cleaved MgO seems to represent an intermediate case.

Figure 10 shows a compilation of RHEED intensity profiles as a function of the substrate temperature  $T_{sub}$ . For this study, Fe<sub>3</sub>O<sub>4</sub>/MgO(100) films annealed for 1 h at 875 K in  $1 \times 10^{-6}$  Pa O<sub>2</sub> were chosen as substrates, because they yielded the most reproducible results. However, we point out that similar trends were observed for deposition onto *ex situ* cleaved and annealed MgO(100) substrates. First of all, we always observe intensity oscillations, indicating that Fe<sub>3</sub>O<sub>4</sub> has a 2D layer-by-layer growth mode over the entire temperature range studied, from 273 to 723 K. From the RHEED patterns, at 273 K we seem to approach the lower limit for layer-by-layer growth. At this temperature, the  $(\sqrt{2} \times \sqrt{2})R45^\circ$  reconstruction, which is characteristic for flat, well-ordered Fe<sub>3</sub>O<sub>4</sub>(100) surfaces (see Sec. III C), is replaced by a 3D transmission pattern. Nevertheless, the period of the oscillations is constant for all substrate temperatures, indicating that even at room temperature, NO<sub>2</sub> is capable of inducing stoichiometric Fe<sub>3</sub>O<sub>4</sub>. This is remarkable because usually  $\sim 475$  K is reported as the lower limit to obtain epitaxial and monophasic films.<sup>14,19,21</sup> Another intriguing feature is that, at 323 K, there is a phase shift between the fifth and fifteenth oscillations.

When  $T_{sub}$  is increased, the number of oscillations increases. They are most persistent between 423 and 473 K. At these temperatures, the damping of the amplitude with deposition time is sometimes so small, that up to several hundreds of oscillations can be observed. For higher temperatures, the intensity profile is characterized by an initial burst of a few very strong oscillations. Furthermore, there is always a phase shift of  $\sim 0.25$ – $0.3$  periods, which manifests itself as an initial increase in intensity. As  $T_{sub}$  approaches 723 K, the amplitude is more rapidly damped, and consequently the number of observable oscillations decreases. The damping of the oscillations does not necessarily imply a transition to a more roughened surface with a growth front that is distributed over several layers—it only indicates a situation where the step density has reached a steady state, without net variations in an area corresponding to the coherence length.<sup>58,59,61</sup>

As  $T_{sub}$  increases, the mobility of the diffusing species will also increase. Therefore, it seems likely that there is a gradual transition from 2D island nucleation to step-flow growth.<sup>63</sup> In step flow, the diffusion length of the atoms is large enough to reach the step edges of neighboring terraces. Consequently, new 2D islands will not be formed anymore, and the step density does not increase. However, the surface still grows in a layer-by-layer like mode. This is in agree-

ment with the RHEED patterns, which show sharp streaks and clear  $(\sqrt{2} \times \sqrt{2})R45^\circ$  reconstructions, indicative of flat and well-ordered surfaces.

Surprisingly, this situation is reversed when  $T_{sub}$  is further raised. For temperatures above  $\sim 700$  K, there is a return to persistent oscillations, with a very large amplitude and small damping. We attribute this behavior to Mg outdiffusion. Probably at 723 K this outdiffusion is so rapid that Mg is constantly appearing at the surface during deposition of new monolayers. Consequently, the film will not be stoichiometric  $Fe_3O_4$  anymore, but  $Mg_xFe_{3-x}O_4$ . The monolayer formation time, however, will not change, because for every Mg ion that diffuses to the surface, one Fe ion has to diffuse to the MgO substrate. We indeed find the same period as for other temperatures. The change from step flow to 2D island nucleation suggests that the diffusion lengths of the migrating species are drastically reduced by the Mg.

Finally, oscillations can be observed for any value of  $\theta$ , i.e., not only in the anti-Bragg position ( $0.68^\circ$ ), but also in random positions, and even in the Bragg position ( $1.36^\circ$ ), similarly to the case of GaAs homoepitaxy.<sup>60</sup> However, the amplitude, mean intensity, and time needed to reach the first maximum all do depend on  $\theta$ . These effects depend critically on the diffraction conditions (azimuthal and polar angle of the electron beam) and can only be explained quantitatively using dynamical scattering theory.<sup>58–60,64</sup> Qualitatively, we report the following trends: The amplitude of the oscillations, with respect to the initial intensity of the specular spot before deposition, increases with decreasing angle of incidence. As mentioned above, oscillations are due to variations in the step density, defined as the step length per unit area. Therefore, this result seems to indicate that the effective step density is larger for smaller angles of incidence. This can be understood if one realizes that the substrate area seen by the electron beam is proportional to  $\sin\theta$ . Secondly, the specular intensity is larger for MgO surfaces than for  $Fe_3O_4$ . Consequently, when  $Fe_3O_4$  is deposited onto MgO, the mean intensity decreases, and vice versa. For  $Fe_3O_4$ /MgO multilayers, this leads to ‘‘block wave’’-like profiles of alternating high and low intensities.<sup>29,65</sup> Finally, the time needed to reach the first maximum *does not* usually correspond to the period of the subsequent oscillations, i.e., there is a phase shift. This effect can best be seen during  $Fe_3O_4$  growth on  $Fe_3O_4$ ; see, for example, curve (d) in Fig. 8. Here, the intensity first increases, to reach a maximum after  $\sim 0.4$  of a full period. Also for NiO and CoO growth on MgO(100), a delay in the first few oscillations has been observed.<sup>23</sup> Such phase shifts, and also the phenomenon of frequency doubling of the oscillations,<sup>60</sup> cannot be explained by interference only. One might argue that, in the case of annealed  $Fe_3O_4$  films, the deposition in the previous experiment was terminated before the last monolayer had been completed. Then, the initial increase in specular intensity in the next experiment would correspond to the completion of this layer. However, as mentioned above, STM images of  $Fe_3O_4$  films have indicated

that all 2D islands are removed by annealing. The resulting surface has large, flat terraces, corresponding to the situation after a completed layer.<sup>27,37</sup>

#### IV. CONCLUSIONS

We have successfully grown single-crystalline, stoichiometric  $Fe_3O_4$  and  $\gamma$ - $Fe_2O_3$  films on MgO(100), using  $NO_2$  as the oxidizing agent. Using Mössbauer spectra of  $^{57}Fe$  probe layers, it was possible to determine accurately the stoichiometry of the films. It is found that all cubic spinel phases can be obtained, i.e., also all intermediate non-stoichiometric  $Fe_{3-\delta}O_4$  phases. The formation of the metastable compound  $\gamma$ - $Fe_2O_3$  clearly demonstrates the large oxidizing power of  $NO_2$ . RHEED and LEED patterns show that the films grow (100)-oriented on MgO(100), with their cubic  $\langle 100 \rangle$  axes aligned parallel to those of the substrate. RBS and XRD measurements reveal a fully coherent or pseudomorphic epitaxial growth; the in-plane lattice constants have fully adjusted to the lattice constant of MgO. Consequently, there are small tetragonal distortions of the unit cells.

Although the shape anisotropy dictates that the magnetization should lie entirely in the plane of the film, this is never observed. Stoichiometric  $Fe_3O_4$  has large out-of-plane components, and only in the case of highly oxidized  $Fe_{3-\delta}O_4$  does the magnetization approach the film plane. However, upon further oxidation to stoichiometric  $\gamma$ - $Fe_2O_3$ , it rotates back, and finally becomes nearly perpendicular to the plane of the film. Furthermore, in the case of (near-) stoichiometric  $Fe_3O_4$ , the magnetizations of the *A* and *B* sublattices are not completely coupled antiparallel. On average, the magnetization of the *B* site ions is  $4^\circ$  closer to the film plane than the magnetization of the *A* site ions.

Oscillations in the intensity of the specularly reflected beam in RHEED give direct, unambiguous evidence that  $Fe_3O_4$  has a 2D layer-by-layer growth mode over the entire temperature range studied, i.e., from 273 to 723 K. The largest oscillations are obtained on *ex situ* cleaved and annealed MgO(100) substrates, or on annealed  $Fe_3O_4$ /MgO(100) films. Deposition above  $\sim 700$  K is accompanied by rapid Mg outdiffusion.

RHEED and LEED diffraction patterns of epitaxially grown  $Fe_3O_4$  and  $\gamma$ - $Fe_2O_3$  films reveal a  $(\sqrt{2} \times \sqrt{2})R45^\circ$  reconstruction of the (100) surface, independent of the stoichiometry. An analysis, based upon electrostatic considerations, indicates three possible surface structures. The first is a termination with a half-filled *A* layer, consisting of one  $Fe^{3+}$  ion per unit cell. The other two are terminations at an oxidized *B* layer, either with oxygen vacancies or hydroxyl groups. Prolonged annealing at high temperatures irreversibly transforms the  $(\sqrt{2} \times \sqrt{2})R45^\circ$  reconstruction into a  $3 \times 1$  reconstruction. XPS spectra indicate that this reconstruction is caused by Mg out diffusion from the substrate.

\*Author to whom correspondence should be addressed. Present address: Laboratory of Electronic Components, Technology and Materials (ECTM), Delft Institute of Microelectronics and Submicron Technology (DIMES), Delft University of Technology, Feld-

mannweg 17, P.O. Box 5053, 2600 GB Delft, The Netherlands. Electronic address: F.C.Voogt@ITS.TUdelft.NL

†Present address: Department of Applied Chemistry, Faculty of Engineering, Okayama University, Tsushima-naka 3-1-1, Okayama

- 700-0082, Japan.
- <sup>1</sup>R. W. G. Wyckoff, *Crystal Structures*, 2nd ed. (Krieger, Malabar, FL, 1982), Vols. 1–3.
  - <sup>2</sup>J.-H. Park, L. H. Tjeng, J. W. Allen, P. Metcalf, and C. T. Chen, *Phys. Rev. B* **55**, 12 813 (1997).
  - <sup>3</sup>J. Smit and H. P. J. Wijn, *Ferrites* (Philips Technical Library, Eindhoven, 1959).
  - <sup>4</sup>P. A. A. van der Heijden, P. J. H. Bloemen, J. M. Metselaar, R. M. Wolf, J. M. Gaines, J. T. W. M. van Eemeren, P. J. van der Zaag, and W. J. M. de Jonge, *Phys. Rev. B* **55**, 11 569 (1997).
  - <sup>5</sup>P. J. van der Zaag, A. R. Ball, L. F. Feiner, R. M. Wolf, and P. A. A. van der Heijden, *J. Appl. Phys.* **79**, 5103 (1996).
  - <sup>6</sup>P. A. A. van der Heijden, P. J. H. Bloemen, J. M. Gaines, J. T. W. M. van Eemeren, R. M. Wolf, P. J. van der Zaag, and W. J. M. de Jonge, *J. Magn. Magn. Mater.* **159**, L293 (1996).
  - <sup>7</sup>F. C. Voogt, T. T. M. Palstra, L. Niesen, O. C. Rogojuanu, M. A. James, and T. Hibma, *Phys. Rev. B* **57**, R8107 (1998).
  - <sup>8</sup>D. T. Margulies, F. T. Parker, M. L. Rudee, F. E. Spada, J. N. Chapman, P. R. Aitchison, and A. E. Berkowitz, *Phys. Rev. Lett.* **79**, 5162 (1997).
  - <sup>9</sup>M. A. M. Gijs and P. J. Kelly, European Patent No. EP 0 672 303 A1 (September 1995).
  - <sup>10</sup>J. M. Daniels and A. Rosenswaig, *J. Phys. Chem. Solids* **30**, 1561 (1969).
  - <sup>11</sup>S. B. Ogale, V. N. Koinkar, Sushama Joshi, V. P. Godbole, S. K. Date, A. Mitra, T. Venkatesan, and X. D. Wu, *Appl. Phys. Lett.* **53**, 1320 (1988).
  - <sup>12</sup>W. F. J. Fontijn, R. M. Wolf, R. Metselaar, and P. J. van der Zaag, *Thin Solid Films* **292**, 270 (1997).
  - <sup>13</sup>W. F. J. Fontijn, P. A. A. van der Heijden, F. C. Voogt, T. Hibma, and P. J. van der Zaag, *J. Magn. Magn. Mater.* **165**, 401 (1997).
  - <sup>14</sup>T. Fujii, M. Takano, R. Katano, Y. Bando, and Y. Isozumi, *J. Appl. Phys.* **66**, 3168 (1989).
  - <sup>15</sup>T. Fujii, M. Takano, R. Katano, Y. Bando, and Y. Isozumi, *J. Cryst. Growth* **99**, 606 (1990).
  - <sup>16</sup>Y. Bando, S. Horii, and T. Takada, *Jpn. J. Appl. Phys.* **17**, 1037 (1978).
  - <sup>17</sup>T. Terashima and Y. Bando, *Thin Solid Films* **152**, 455 (1987).
  - <sup>18</sup>Y. J. Kim, Y. Gao, and S. A. Chambers, *Surf. Sci.* **371**, 358 (1997).
  - <sup>19</sup>R. M. Wolf, A. E. M. De Veirman, P. van der Sluis, P. J. van der Zaag, and J. B. F. aan de Stegge, *Epitaxial Oxide Thin Films and Heterostructures*, edited by D. K. Fork, J. M. Phillips, R. Ramesh, and R. M. Wolf, MRS Symposia Proceedings No. 341 (Materials Research Society, Pittsburgh, 1994), p. 23.
  - <sup>20</sup>T. Siegrist, D. A. Mixon, E. Coleman, and T. H. Tiefel, *Appl. Phys. Lett.* **60**, 2489 (1992).
  - <sup>21</sup>D. M. Lind, S. D. Berry, G. Chern, H. Mathias, and L. R. Testardi, *Phys. Rev. B* **45**, 1838 (1992).
  - <sup>22</sup>K. Norimoto, R. Sekine, M. Mori, T. Hanada, M. Kudo, and M. Kawai, *Appl. Phys. Lett.* **61**, 1971 (1992).
  - <sup>23</sup>S. D. Peacor and T. Hibma, *Surf. Sci.* **301**, 11 (1993).
  - <sup>24</sup>T. Fujii, D. Alders, F. C. Voogt, T. Hibma, B. T. Thole, and G. A. Sawatzky, *Surf. Sci.* **366**, 579 (1996).
  - <sup>25</sup>C. Duriez, C. Chapon, C. R. Henry, and J. M. Rickard, *Surf. Sci.* **230**, 123 (1990).
  - <sup>26</sup>M. Gajdardziska-Josifovska, P. A. Crozier, and M. R. Cartney, *Surf. Sci.* **284**, 186 (1993).
  - <sup>27</sup>J. F. Anderson, M. Kuhn, U. Diebold, K. Shaw, P. Stoyanov, and D. Lind, *Phys. Rev. B* **56**, 9902 (1997).
  - <sup>28</sup>L. H. Tjeng, A. R. Vos, and G. A. Sawatzky, *Surf. Sci.* **235**, 269 (1990).
  - <sup>29</sup>M. A. James, F. C. Voogt, L. Niesen, O. C. Rogojuanu, and T. Hibma, *Surf. Sci.* **402-404**, 332 (1998).
  - <sup>30</sup>T. Fujii, M. Takano, R. Katano, Y. Isozumi, and Y. Bando, *J. Magn. Magn. Mater.* **130**, 267 (1994).
  - <sup>31</sup>T. Fujii, F. M. F. de Groot, G. A. Sawatzky, F. C. Voogt, T. Hibma, and K. Okada, *Phys. Rev. B* **59**, 3195 (1999).
  - <sup>32</sup>F. C. Voogt, T. Fujii, T. Hibma, M. Hoefman, P. J. M. Smulders, G. H. Wijnja, G. L. Zhang, and L. Niesen, *Hyperfine Interact.* **97/98**, 99 (1996).
  - <sup>33</sup>F. C. Voogt, T. Hibma, P. J. M. Smulders, and L. Niesen, *J. Cryst. Growth* **174**, 440 (1997).
  - <sup>34</sup>F. C. Voogt, T. Hibma, P. J. M. Smulders, L. Niesen, and T. Fujii, in *Epitaxial Oxide Thin Films III*, edited by D. G. Schlom *et al.*, MRS Symposia Proceedings No. 474 (Materials Research Society, Pittsburgh, 1997), p. 211.
  - <sup>35</sup>F. C. Voogt, T. Hibma, P. J. M. Smulders, L. Niesen, T. Fujii, P. A. A. van der Heijden, R. J. M. van de Veerdonk, and P. J. van der Zaag, *J. Phys. IV* **7**, C1-601 (1997).
  - <sup>36</sup>C. A. Kleint, H. C. Semmelhack, M. Lorenz, and M. K. Krause, *J. Magn. Magn. Mater.* **140-144**, 725 (1995).
  - <sup>37</sup>J. M. Gaines, P. J. H. Bloemen, J. T. Kohlhepp, C. W. T. Bulle-Lieuwma, R. M. Wolf, A. Reinders, R. M. Jungblut, P. A. A. van der Heijden, J. T. W. M. van Eemeren, J. aan de Stegge, and W. J. M. de Jonge, *Surf. Sci.* **373**, 85 (1997).
  - <sup>38</sup>D. T. Margulies, F. T. Parker, F. E. Spada, R. S. Goldman, J. Li, R. Sinclair, and A. E. Berkowitz, *Phys. Rev. B* **53**, 9175 (1996).
  - <sup>39</sup>R. Bauminger, S. G. Cohen, A. Marinov, S. Ofer, and E. Segal, *Phys. Rev.* **122**, 1447 (1961).
  - <sup>40</sup>J. M. D. Coey, A. H. Morrish, and G. A. Sawatzky, *J. Phys. C* **32**, C1-271 (1971).
  - <sup>41</sup>G. A. Sawatzky, F. van der Woude, and A. H. Morrish, *Phys. Rev.* **183**, 383 (1969).
  - <sup>42</sup>L. Häggström, H. Annersten, T. Ericsson, R. Wäppling, W. Karner, and S. Bjarman, *Hyperfine Interact.* **5**, 201 (1978).
  - <sup>43</sup>T. Fujii, M. Takano, R. Katano, Y. Bando, and Y. Isozumi, *J. Appl. Phys.* **68**, 1735 (1990).
  - <sup>44</sup>S. A. Chambers and S. A. Joyce, *Surf. Sci.* **420**, 111 (1999).
  - <sup>45</sup>P. J. H. Bloemen, P. A. A. van der Heijden, R. M. Wolf, J. aan de Stegge, J. T. Kohlhepp, A. Reinders, R. M. Jungblut, P. J. van der Zaag, and W. J. M. de Jonge, *Epitaxial Oxide Thin Films II*, edited by D. K. Fork, G. S. Speck, T. Shiusaki, and R. M. Wolf, MRS Symposia Proceedings No. 401 (Materials Research Society, Pittsburgh, 1996), p. 485.
  - <sup>46</sup>N. N. Greenwood and T. C. Gibb, *Mössbauer Spectroscopy* (Chapman and Hall, London, 1971).
  - <sup>47</sup>G. Tarrach, D. Bürgler, T. Schaub, R. Wiesendanger, and H.-J. Güntherodt, *Surf. Sci.* **285**, 1 (1993).
  - <sup>48</sup>F. C. Voogt, T. Hibma, G. L. Zhang, M. Hoefman, and L. Niesen, *Surf. Sci.* **331-333**, 1508 (1995).
  - <sup>49</sup>P. A. A. van der Heijden, J. J. Hammink, P. J. H. Bloemen, R. M. Wolf, M. G. van Opstal, P. J. van der Zaag, and W. J. M. de Jonge, *Magnetic Ultrathin Films, Multilayers, and Surfaces*, edited by A. Feit, H. Fujimori, G. Guntherodt, B. Heinrich, W. F. Egelhoff, Jr., E. E. Marinero, and R. C. White, MRS Symposia Proceedings No. 384 (Materials Research Society, Pittsburgh, 1995), p. 27.
  - <sup>50</sup>A. Barbieri, W. Weiss, M. A. Van Hove, and G. A. Somorjai, *Surf. Sci.* **302**, 259 (1994).
  - <sup>51</sup>P. W. Tasker, *J. Phys. C* **12**, 4977 (1979).

- <sup>52</sup>M. D. Pashley, Phys. Rev. B **40**, 10 481 (1989).
- <sup>53</sup>R. Wiesendanger, I. V. Shvets, D. Bürgler, G. Tarrach, H. J. Güntherodt, J. M. D. Coey, and S. Gräser, Science **255**, 583 (1992).
- <sup>54</sup>C. R. Brundle, T. J. Chuang, and K. Wandelt, Surf. Sci. **68**, 459 (1977).
- <sup>55</sup>J. M. Gaines, J. T. Kohlhepp, J. T. W. van Eemeren, R. J. G. Elfrink, F. Roozeboom, and W. J. M. de Jonge, in *Epitaxial Oxide Thin Films III* (Ref. 34), p. 191.
- <sup>56</sup>H. C. Galloway, P. Sautet, and M. Salmeron, Phys. Rev. B **54**, R11 145 (1996).
- <sup>57</sup>J. H. Neave, B. A. Joyce, P. J. Dobson, and N. Norton, Appl. Phys. A: Solids Surf. **31**, 1 (1983).
- <sup>58</sup>B. A. Joyce, J. Cryst. Growth **99**, 9 (1990).
- <sup>59</sup>J. Zhang, J. H. Neave, B. A. Joyce, P. J. Dobson, and P. N. Fawcett, Surf. Sci. **231**, 379 (1990).
- <sup>60</sup>J. Zhang, J. H. Neave, P. J. Dobson, and B. A. Joyce, Appl. Phys. A: Solids Surf. **42**, 317 (1987).
- <sup>61</sup>J. Sudijono, M. D. Johnson, C. W. Snyder, M. B. Elowitz, and B. G. Orr, Phys. Rev. Lett. **69**, 2811 (1992).
- <sup>62</sup>S. S. Kim, S. Baik, H. W. Kim, and C. Y. Kim, Surf. Sci. **294**, L935 (1993).
- <sup>63</sup>T. Shitara, D. D. Vvedensky, M. R. Wilby, J. Zhang, J. H. Neave, and B. A. Joyce, Phys. Rev. B **46**, 6815 (1992).
- <sup>64</sup>Y. Horio and A. Ichimiya, Surf. Sci. **298**, 261 (1993).
- <sup>65</sup>G. Chern and Y. R. Chean, J. Appl. Phys. **36**, 2813 (1997).